An Integrated Laser Trap/Flow Control Video Microscope for the Study of Single Biomolecules

Gijs J. L. Wuite,* R. John Davenport,[†] Aaron Rappaport,[‡] and Carlos Bustamante*[†]

[‡]Institute of Molecular Biology, University of Oregon, Eugene, Oregon 97403, and [†]Department of Molecular and Cell Biology and *Department of Physics, University of California, Berkeley, California 94720 USA

ABSTRACT   We have developed an integrated laser trap/flow control video microscope for mechanical manipulation of single biopolymers. The instrument is automated to maximize experimental throughput. A single-beam optical trap capable of trapping micron-scale polystyrene beads in the middle of a 200-μm-deep microchamber is used, making it possible to insert a micropipette inside this chamber to hold a second bead by suction. Together, these beads function as easily exchangeable surfaces between which macromolecules of interest can be attached. A computer-controlled flow system is used to exchange the liquid in the chamber and to establish a flow rate with high precision. The flow and the optical trap can be used to exert forces on the beads, the displacements of which can be measured either by video microscopy or by laser deflection. To test the performance of this instrument, individual biotinylated DNA molecules were assembled between two streptavidin beads, and the DNA elasticity was characterized using both laser trap and flow forces. DNA extension under varying forces was measured by video microscopy. The combination of the flow system and video microscopy is a versatile design that is particularly useful for the study of systems susceptible to laser-induced damage. This capability was demonstrated by following the translocation of transcribing RNA polymerase up to 650 s.

INTRODUCTION

Since its demonstration by Arthur Ashkin in 1986 (Ashkin et al., 1986), the optical trap has become an increasingly important tool in biophysics and cell biology. Experimental laser trapping techniques have been used to directly manipulate and trap cells, organelles inside cells, and viruses (Kuo and Sheetz, 1992; Ashkin and Dziedzic, 1987). In addition, optical trapping, combined with microsphere handles linked to molecules of interest, has been used to measure the force-producing properties of various biological systems, including kinesin moving along microtubules (Svoboda et al., 1993), actomyosin complexes (Finer et al., 1994), RNA polymerase (Davenport et al., 2000; Wang et al., 1998; Yin et al., 1995), and DNA polymerase (Wuite et al., 2000), as well as to measure the elastic properties of DNA (Cluzel et al., 1996; Smith et al., 1996) and the giant muscle protein titin (Kellermayer et al., 1997; Tskhovrebova et al., 1997).

Optical traps can stably trap particles of a wide range of sizes, from diameters much smaller than the wavelength of light (Rayleigh-size regime) to diameters much larger than the wavelength of light (ray optics regime). The size of particles manipulated in many biophysical applications of optical trapping microscopy are on the order of the wavelength of light and therefore fall between these two regimes. A theoretical description of trapping in this intermediate regime is difficult. Ray optics can nonetheless be used to obtain a qualitative model of the two main forces acting on intermediate-size beads (Ashkin, 1992). One force is largely

due to backscattering of photons by the sphere and tends to push it down the optical axis; this force is often referred to as the *scattering force*, F_{scat}. A second force, the *intensity gradient force*, F_{grad}, tends to pull the object in the direction of increasing intensity of the beam. For a laser beam focused by a high-numerical-aperture lens, a substantial intensity gradient develops perpendicular to the beam axis, as well as along the beam axis, pulling the bead toward the focus and counteracting the backscattering force. When these forces balance each other, a dielectric object can be held at a stable position just downstream of the objective focus.

The forces involved in many biological processes fall within the range that can be exerted by an optical trap. For instance, the reported stalling forces for kinesin, myosin, RNA polymerase, and DNA polymerase are 5–6 pN (Svoboda et al., 1993), 3.5 pN (Finer et al., 1994), 14–25 pN (Davenport et al., 2000; Wang et al., 1998; Yin et al., 1995), and 34 pN (Wuite et al., 2000), respectively. Force-induced structural transition in nucleic acids (Cluzel et al., 1996; Smith et al., 1996) or proteins (Kellermayer et al., 1997; Tskhovrebova et al., 1997) require forces up to 80 pN or so. These forces can be measured by optical trapping techniques, because for a small external force a trapped object is displaced a distance proportional to that force. This displacement (and hence the external force) can be measured by detecting corresponding changes in the polarization of the laser beam (Denk and Webb, 1990; Svoboda et al., 1993) or deflection of the laser beam by the use of photodiodes (Davenport et al., 2000; Ghislain et al., 1994; Smith et al., 1996).

Hydrodynamic flow has also been successfully used to apply forces to single molecules. For instance, the dynamic response of single DNA molecules to a hydrodynamic drag force has been studied in laminar flows (Perkins et al., 1997; Smith and Chu, 1998). The force-extension behavior of

DNA has been characterized with a combination of magnetic and drag forces on beads tethered to DNA (Smith et al., 1992). Because laminar flows are used to generate forces in these single-molecule studies, drag forces can be calculated using Stokes' law. For any size sphere in water, Stokes' law remains valid for forces up to 10 nN, at which point the Reynolds' number exceeds unity. Single-molecule experiments are almost always carried out in the confined space of a sample chamber. Therefore, force determination should take into account the modification of Stokes' law due to the hydrodynamic coupling between the bead and the boundaries of the microchamber (Happel and Brenner, 1991; Lorentz, 1907; Smith et al., 1992).

Both optical trapping and flow control systems represent important technical developments in biophysics that are readily applicable to the study of single-molecule mechanics and force-generating systems. Moreover, these methods have complementary features: laser traps afford excellent spatial resolution and force control, but can induce radiation damage in the samples. Problems also arise from the use of oil immersion objective lenses, which form optical traps near the surface of the sample chamber. Calibration of such traps is difficult because small changes in distance from the coverslip result in large differences in hydrodynamic coupling of the beads to the glass surface and in trap stiffness due to spherical aberration. Hydrodynamic flows, on the other hand, greatly extend the range of forces that can be applied with laser traps, without inducing radiation damage. However, video detection combined with flow systems has lower spatial resolution and reduced force control as compared to laser trapping detection systems. In addition, there are experimental drawbacks common to the two techniques. In both setups, experiments in which molecules are tethered to the glass surface of the fluid chamber require setting up a new chamber each time the experimental sample has become inactive or unusable, increasing experimental times and reducing overall throughput. Furthermore, if a polymer molecule is attached to a surface and aligned at an angle to the vector of force application, a further correction for this angle must be made. One solution of this problem was offered by Ishijima et al. (1998), who used a surface with a microfabricated pedestal.

It is therefore advantageous to design and build an instrument that combines the complementary capabilities of both optical trapping and hydrodynamic flow control while being easy to calibrate, having improved experimental geometry, faster data throughput, and controllable laser exposure. We communicate here the design of an integrated laser trap/flow control video microscope that is automated to maximize its throughput in single-biomolecule experiments. This instrument was previously used in the study of RNA polymerase by Davenport et al. (2000). This instrument can be used in one of three operation modes: 1) laminar flow mode, where forces are exerted through the hydrodynamic drag experienced by a bead and the bead positions are determined by video microscopy; 2) laser trap mode, where the laser power is used both to exert force on the bead and to determine the bead position; and 3) combined laminar/optical mode, in which the force is exerted both hydrodynamically and optically, but the bead position is tracked by the laser beam, at high or low power. The use of exchangeable beads in this design greatly decreases the experimental setup times. Surface effects are minimized by trapping these beads deep inside the microchamber, through the use of a water immersion, long-working-distance objective. Finally, through the use of either the laminar flow mode or the combined mode, radiation damage can be minimized. Two experiments illustrate the versatility of this system. The elasticity of DNA was characterized by using both the combined mode and the laminar flow mode. Furthermore, transcriptional translocation by RNA polymerase was followed over long times without radiation damage, using the laminar flow mode.

INSTRUMENTAL DESIGN

Optics

The optics of the laser trap/flow control video microscope are depicted in Fig. 1. The optical trap in this instrument can stably trap refractive objects far from the cover slide (up to 150 μm) with a single laser beam. This capability results from the use of a high numerical aperture water immersion objective lens, which has much less spherical aberration than an oil immersion objective (Brenner, 1994). This type of objective is commonly used for imaging through thick water layers or thick samples (Perkins et al., 1997; Smith and Chu, 1998). High NA oil immersion objectives are commonly used to generate high-angle peripheral rays, which are necessary to create a refractive force capable of counteracting the backscattering force on a dielectric object. An oil immersion lens forms a stiffer trap close to a surface than is possible with a water immersion objective. Deeper inside the sample chamber, however, rays are not directed toward a single focus, and an optical trap formed by an oil immersion lens rapidly decreases in stiffness. Particles can no longer be stably trapped at distances beyond several microns from the surface (e.g., a 1-μm polystyrene sphere cannot be trapped at a depth greater than 21 μm from the surface; Ghislain et al., 1994). A single beam optical trap that uses a water immersion, high-NA objective (typically 1.2) can be used to focus the axial and peripheral rays to the same focus both close to and far away from the coverglass (Davenport et al., 2000). As a result, the trap stiffness is independent of the relative distance between the trap and the coverslide surface. Dual beam traps, which use two counterpropagating, confocal laser beams, suffer from spherical aberration as well, but the gradient forces dominate because the scattering forces of the two beams cancel. Therefore they can trap objects stably far from the glass surface, using low numerical aperture lenses (Smith et al., manuscript in
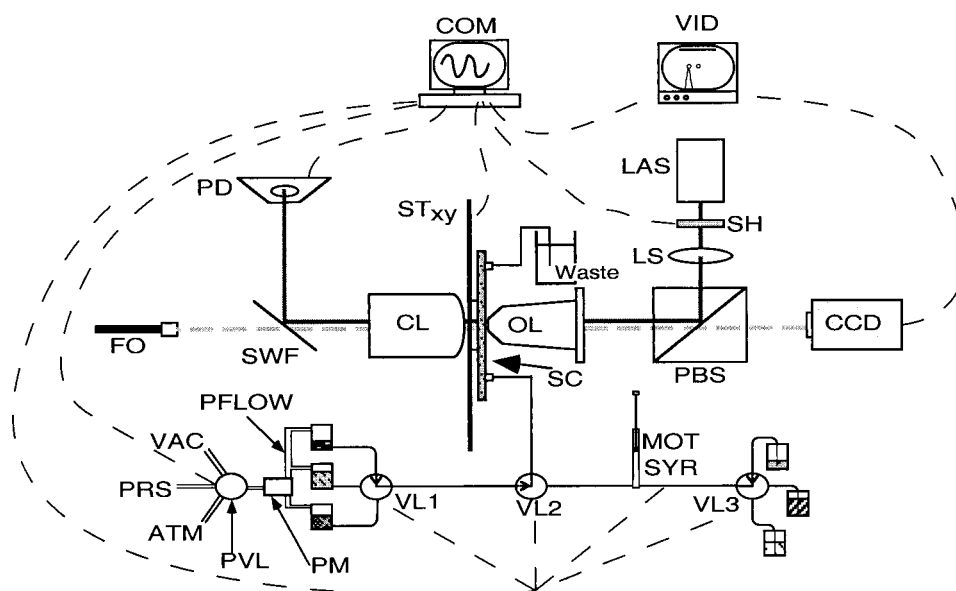
FIGURE 1 Schematic of integrated optical trapping/flow control video microscope. The optical trapping microscope is constructed horizontally on an optical breadboard (Newport Research Corporation, Irvine, CA) and suspended by elastic shock cords. Commercial microscope configurations have been avoided to minimize undesirable mechanical vibration. The laser beam (LAS) (from a single-mode, circular corrected, linearly polarized diode, $\lambda = 835$ nm, 178 mW maximum power; Melles Griot, Boulder, CO) passes through a computer-controlled shutter (SH) (Melles Griot), is reflected by a broadband polarizing beamsplitter cube (PBS), and is focused (LS) 160 mm upstream from the objective lens. The objective, a water immersion, high numerical aperture (NA) lens (OL) (PlanApo 60, NA = 1.2, Nikon; Meridian Instruments, Okemos, MI) focuses the laser beam in the middle of a 200-μm-deep sample chamber (SC). The working distance of the objective is 220 μm from the coverslide surface. The exiting laser light is collected by a large-aperture oil immersion condenser (CL). The beam is then reflected by a short wave pass filter (SWF) (SPF 650; CVI Laser Corp., Albuquerque, NM) onto a 2D position-sensitive photodetector (PD) (DL10; UDT Sensors, Hawthorne, CA). A fiber optic visible light source (FO) (Tri-Lite; World Precision Instruments, Sarasota, FL) propagating in the direction opposite that the laser beam is used to illuminate the sample. The image formed in transmission by the objective is then projected through a beamsplitting cube onto a CCD camera (CCD) (Watec monochrome CCD; Edmund Scientific, Barrington, NJ). Polyethylene tubing (ID = 0.28 mm, OD = 0.61 mm; Becton Dickinson, Sparks, MD) and flangeless fittings (Upchurch Scientific, Oakharbor, WA) are used to connect all components of the flow system. The total dead volume between the pressure bottles (PFLOW) and the middle of the sample chamber is $\sim$ 55 μl. The pressure in the bottles is regulated by three computer-controlled solenoid valves (PVL) (Clippard, Cincinnati, OH): one is connected to a $+0.5$-atm pressure source (PRS), another to a -0.5-atm vacuum (VAC), and the third to atmospheric pressure (ATM). The pressure or vacuum solenoid valve is opened for $\sim$7 ms to incrementally increase or decrease, respectively, the pressure in the line; this in turn increases or decreases the rate of buffer flow through the chamber. Buffer flow is stopped by opening the atmosphere solenoid valve. The pressure exerted on the solutions in the bottles is monitored by the computer via a pressure transducer (accuracy $\pm 0.1\%$). The instrument functions and data collection are controlled by the personal computer (COM) (Intel 486, 66 MHz; Comtrade, City of Industry, CA) and custom-written software. The computer controls the position of the sample chamber via an internal I/O card (CIO-DIO96; Computer Boards, Mansfield, MA) connected to custom-built digital-to-analog converters. The signal from these converters modulates the voltage output of 1000-V power operational amplifiers (BOP-1000M; Kepco, Flushing, NY), which control the x and y piezo actuators (40 μm piezos; Burleigh, Fisher, NY) on the flexure stage (STxy). To allow for a larger degree of automation in this instrument, the I/O card also interfaces between a variety of other components of the instrument, including a piezoelectric controller (MDT691; Thorlabs, Newton, NJ), which allows computer control of the objective focus via a piezoelectric actuator (PA) (PE4; Thorlabs), the shutter, and the pressure solenoid valves. The CCD camera is connected through a video monitor (VID) to a video board (DT55–60; Data Translation, Marlboro, MA) in the computer. The camera and the video board are used to determine the position and size of objects in the video image (bandwidth 60 Hz; maximum sample frequency 30 Hz). An analog-to-digital converter card (DAS-802; Keithley, Taunton, MA) is used for data collection from the photodetector and from the pressure meter. The selector valves (VL 1, 2, and 3) (MVP modular positioner; Hamilton, Reno, NV) and the automatic syringe (MOT SYR) (PSD/2; Hamilton) are connected in a daisy chain to the computer parallel port. Liquids from the bottles controlled by selector valve 3 are introduced into the fluid chamber with the automatic syringe, which functions as a pump.

preparation). Dual beam traps, however, are somewhat difficult to align and are more sensitive to optical drift. The single-lens design is easy to set up and align.

Micropipette and exchangeable surfaces

Trapping objects deep inside the sample chamber makes the introduction of a micropipette possible (Fig. 2). A bead held by suction on the tip of the pipette can be used as an easily exchangeable surface of well-defined chemical properties to which molecules can be attached. With the use of beads as replaceable attachment surfaces, many single-molecule experiments can be performed without replacing the entire fluid chamber. Moreover, this design can easily be adapted to a large variety of molecular systems by simply changing the chemistry of the beads or appropriately labeling macromolecules.

The assembly of macromolecules between beads can be performed in a very controlled fashion by using a two-bead
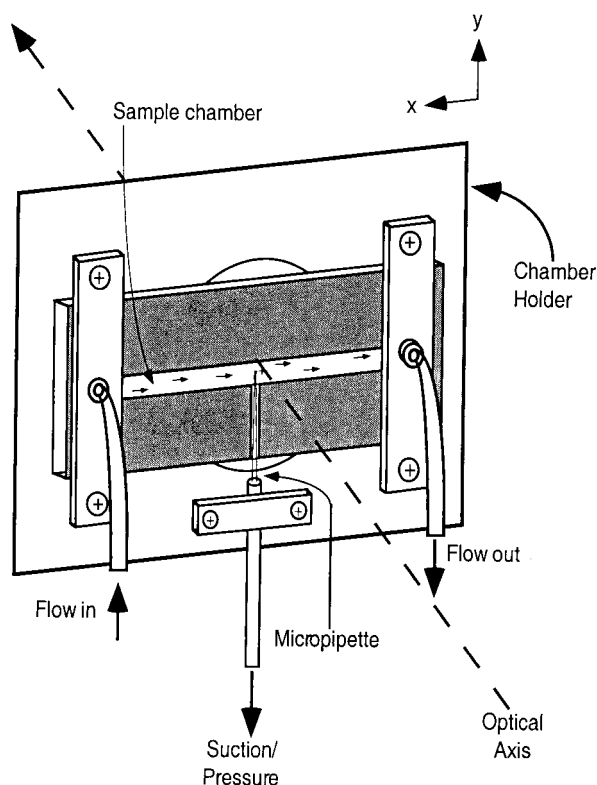
FIGURE 2 The sample chamber is assembled by placing two layers of parafilm cut in the chamber shape between a microscope slide and a coverglass. The chamber is sealed to withstand the fluid pressure by heating the two parafilm layers that are pressed between the slide and the coverglass. A 100-μm-inner diameter quartz catheter tube is placed between the two layers of parafilm to allow the introduction of a micropipette into the chamber. Two holes drilled through the coverglass form the entrance and exit ports for the flow chamber. The chamber is clamped on a holder by two aluminum brackets that have threaded holes to connect tubing to the chamber by means of flangeless fittings. Micropipettes are pulled from glass capillaries (ID = 40 $\pm$ 6.4 μm, OD = 80 $\pm$ 6.4 μm, KG-33 glass; Garner Glass Co., Claremont, CA) in a hand-built resistance element/gravity pipette puller. The final pipette internal diameter varies from 0.5 to 1 μm tapered over ~1.5–2 mm. The pipettes are glued into polyethylene tubing (ID = 0.28 mm), using UV-curing epoxy (Norland Products, New Brunswick, NJ). Polystyrene beads of 1–10 μm diameter can be held on the tip of the pipette by suction. The pipettes are introduced into the sample chamber through the catheter tube and clamped on the sample chamber holder with a Plexiglas bracket. The catheter tube is sealed with agarose to prevent leakage of fluid from the chamber. A syringe attached to the other end of the tubing is used to apply suction and pressure in the pipette. At the end of the usable lifetime of a pipette, a new chamber can be constructed or the micropipette in the existing chamber can be replaced. The sample chamber itself is mounted on a custom-built x-y flexure stage driven by 40-μm piezos. The position of the stage is under computer control and moves the pipette relative to the fixed position of the laser trap in the plane perpendicular to the optical axis. The relative z positions of the optical trap and the pipette are controlled by the z position of the focus of the objective.

design. We have attached single biomolecules between a bead in the trap and a bead on the pipette as depicted in Fig. 3. At the beginning of an experiment, streptavidin-coated
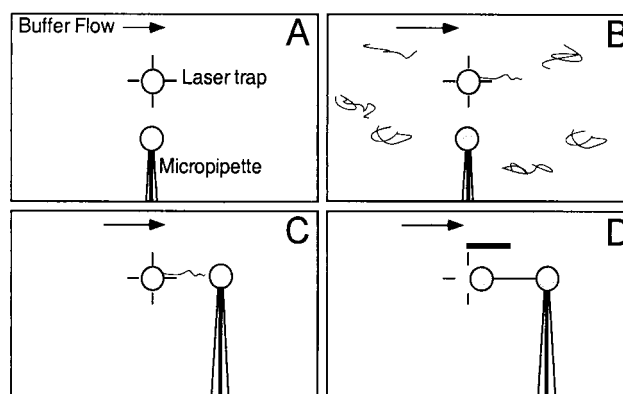

FIGURE 3 Assembly of DNA and DNA-protein complexes. (*A*) To start an experiment, polystyrene beads modified for a specific biological experiment are allowed to flow into the fluid chamber. One bead is held on the tip of the micropipette by suction and one is held in the laser trap. (*B*) Macromolecules (i.e., DNA or stalled transcription complexes; Appendix A) flow in, and their appropriately modified ends can attach to the beads. Upon attachment the DNA is stretched out in the flow because of the drag force experienced by the beads. (*C*) The bead on the tip of the pipette is moved close to the bead in the trap to attach the free end of the macromolecule to the bead in the trap. (*D*) An attachment can be confirmed when the bead in the trap experiences a fast increase of force over a short distance. Once an attachment is made, measurements can be taken.

polystyrene microspheres are injected into the fluid chamber, and when the laser trap is turned on, one such bead is captured by the trap. Next, the pipette is brought close to the trap and the bead in the trap is transferred to the tip of the micropipette. A second bead is then captured in the laser trap. With a bead on the micropipette and one in the laser trap, appropriately labeled molecules (either linear DNA with biotin tags at either end or biotinylated transcription complexes for the applications demonstrated here; Appendix A) are introduced into the flow chamber. When one end of a molecule attaches to the bead, the molecule extends by viscous drag in the direction of the flow (Fig. 4). The pipette bead can then be moved near the trapped bead to promote attachment of the free end of a molecule to its surface (Appendix A). This procedure can be used for a wide range of biopolymer lengths; DNA molecules as small as 100 nm have been tethered between beads.

During the tethering process of force-sensitive biological systems such as RNA polymerase between two beads, care must be taken to avoid irreversible damage to the molecule by minimizing the force applied to it. To this end, the tethering procedure described above has been completely automated and is controlled by the computer. During the procedure, the computer controls the back and forth movement of the pipette bead relative to the trapped bead via the fine piezo control of the stage position, while the force on the trapped bead is monitored by the computer. When a tether is formed the bead is displaced from the center of the trap and experiences a sudden increase in force. Because the
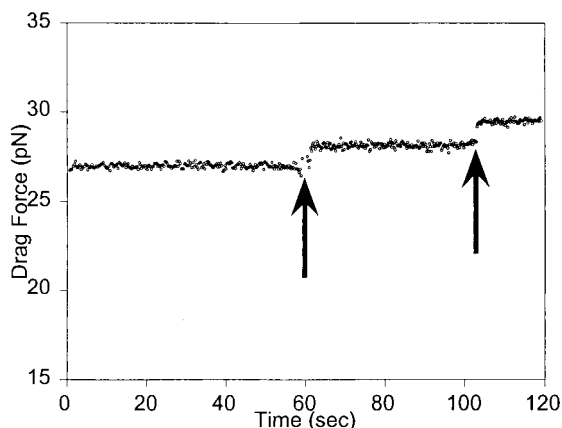
FIGURE 4 A micron-sized bead is kept in a laser trap while ~10-kb-long DNA molecules pass through the fluid chamber. Upon connection of a biotinylated DNA molecule to the streptavidin on the beads, the measured drag force of the bead increases (↑). This distinct increase in drag allows precise knowledge of the number of molecules attached to the bead.

computer can monitor this force change with higher precision than a manual operator can, the automated procedure limits the maximum force experienced by the molecule to <10 pN (manual tethering >20 pN). In addition to minimizing the applied force, the computer-controlled procedure is less error prone than it would be if it were carried out manually, and thus it increases molecule assembly throughput.

There are some drawbacks to the use of a micropipette. The tip of the pipette is very fragile and can easily be damaged if it is handled outside the chamber. Inside the chamber, however, it can be used over many months by rinsing the chamber and pipette with distilled, deionized water after use and storing them dry to prevent bacterial contamination. Another problem is that a bead held by suction does not always seal the pipette tip completely. This introduces a residual suction that can disrupt an experiment (i.e., a DNA molecule tethered between two beads can be sucked into the pipette). This problem can easily be overcome by decreasing the vacuum in the pipette to only the amount necessary to keep the bead on the pipette. This greatly diminishes the residual suction of the pipette when it is not sealed entirely. While a second optical trap could be substituted for the pipette, a pipette is much stiffer (~4 nN/μm) than an optical trap. In addition, forces of 150 pN or more do not dislodge a bead held on the pipette by suction. Thus the pipette functions as a stationary wall.

Flow system

Flow and buffer exchange in the sample chamber are controlled via an automated syringe, pressure bottles, and automated selector valves (Fig. 1). The automated syringe is used to inject volumes of suspended beads, to clean the chamber, and to remove air bubbles from the flow system.

Buffer flow from the pressure bottles is achieved by hydrostatic pressure on the buffer. A desired buffer is selected by connecting that pressure bottle to the buffer line entering the chamber via the automated selector valves. The fluid waste exits the chamber and is disposed in a container. The three selector valves can be used to program automatic cycles of buffer exchange through the chamber.

The flow rate is linear with applied pressure and vacuum (Fig. 5 A) and is capable of producing hydrodynamic drag forces up to 100 pN on a 1.1-μm-radius bead in both the forward and backward flow directions. Flow speeds used in this instrument are less than 4000 μm/s, using 1.1-μm beads (2.4 μl/s). The total volume of fluids in the pressure bottles (~4 ml) is small compared with the volume of air in the pressure system (~80 cc), and the average flow rates used in this system are small (~1 μl/s). Therefore, the change in
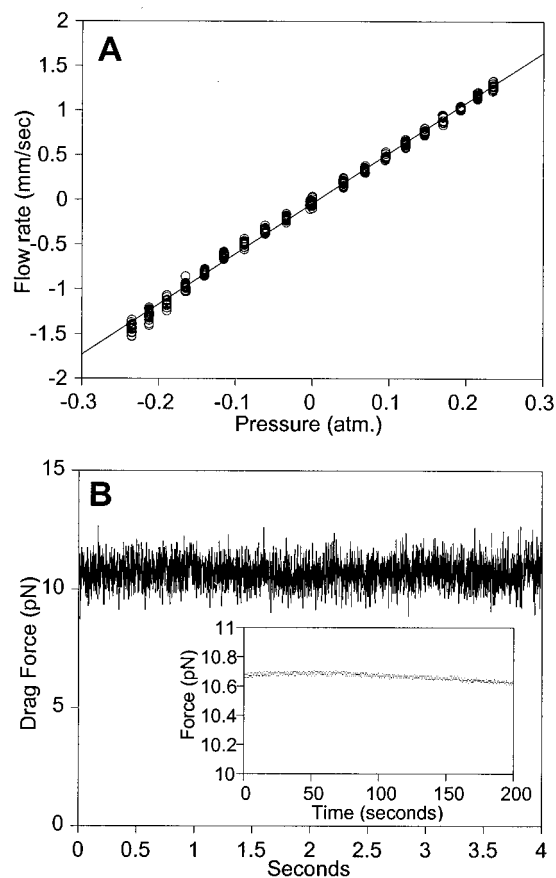

FIGURE 5 (A) At each pressure, the flow speed is measured as described for the flow speed calibration. The flow speed is linear with applied pressure and suction. (B) A 2.2-μm bead is trapped in a 178-mW laser beam while a flow is applied through the fluid chamber. Analysis of short-term flow stability: data were taken at a 1-kHz sample rate. The drag force experienced by the bead is 10.6 pN. The Brownian motion of the trapped bead causes a 0.6-pN fluctuation (RMS value) or ~6 nm (X_{rms}, $\alpha_{DNA} = 110$ pN/μm). Inset: Long-term flow stability. The data points are averaged over a 0.2-s period. The fluctuation in drag force is on the order of ~0.04 pN.

gas volume due to displaced fluid is small, and the flow is stable over many minutes (Fig. 5 *B*). Moreover, the flow rate can be ramped by increasing or decreasing the pressure. Sets of buffer bottles for different experiments are contained on easily exchangeable fluid cartridges, making the transfer between new experimental conditions rapid and efficient.

Position and force detector

For the high-resolution detection of bead displacements and forces we use the laser deflection method of Ghislain et al. (Ghislain et al., 1994; Ghislain and Webb, 1993), except that a 2D lateral effect position detector is used instead of a single photodiode. This detector determines the weighted average center of mass of the laser spot on the detector in two dimensions. Unlike the method of Ghislain et al., the active area of the detector is larger than the intercepted laser beam and thus is insensitive to bead movements along the optical axis. A microscope condenser collects the exiting light after it is refracted by the trapped bead. The condenser lens casts the laser beam directly on the 2D position detector, which is placed on the optical axis far behind the intermediate image plane, so that the defocused laser beam is ~0.8 cm^2, somewhat smaller than the size of the detector. Bead displacements relative to the fixed position of the optical trap deflect the laser beam on the detector. Placing the detector behind the image plane instead of in the back-focal plane makes the detector sensitive to translations of the *x-y* position of the optical axis, which can be considered a drawback of this method (Gittes and Schmidt, 1998; Visscher et al., 1996). The position-sensitive detector employed here has instrumental noise comparable to that of interferometry-based systems (~0.015 nm/Hz$^{1/2}$) while having sensitivity in two dimensions. The position-sensing photodetector also has advantages over a quadrant detector because it has a larger linear range than the latter and is less sensitive to changes in the shape and size of the projected beam. However, it is slower ($B = $ ~100 kHz) and somewhat less sensitive than a quadrant detector.

The instrument described here uses a diode laser; these lasers suffer from "mode hopping" (frequency shifting), which includes beam pointing instabilities. Mode hopping arises from temperature fluctuations at the junction in the diode and can create an artificial shift in the bead position measurement. However, diode lasers are convenient because diode temperature can be well controlled with a thermoelectric cooler (resolution ± ~0.01°C). Moreover, antireflection coatings that reduce back-reflections can be used to further minimize mode hopping.

The output from the position-sensitive detector is converted into *x* position, *y* position, and total intensity signals by a custom-built analog electronics board. We used a feedback resistor of 15 kΩ in this current-to-voltage circuit, which gave a good compromise between resistor noise and gain, because the direct laser light on the detector induces a strong signal (~mA) (the detector responsivity is 0.55 mA/mW at 835 nm). For flexibility, the deflection signal is normalized to the total intensity with software if desired. The signal is low-pass filtered by analog electronics before sampling. This low-pass frequency is equal to the Nyquist frequency (f_{nyq}) for the sample rate used ($f_s = 2f_{nyq}$) (Horowitz and Hill, 1989). The low-pass frequency can easily be altered in our electronics by using different capacitors, creating flexibility in the sampling rate ($f_s = $ 0.1–2 kHz).

Automation

The throughput of this instrument has been maximized, in part by extensive automation of many instrument functions. Automation reduces operator error and ensures that procedures are repeated exactly from experiment to experiment. In particular, functions that are required for multiple buffers flowing through the sample chamber can be preprogrammed. These functions include injection of beads, changing buffers during experiments, washing out the chamber at the end of an experiment to initiate a new one, and eliminating air bubbles from the flow system. Other instrumental functions such as calibration of flow rates, position, and force calibration of the photodetector and the determination of the stiffness of the trap are also fully automated. Many operations required to assemble molecules between a bead in the trap and a bead on the micropipette are also automated and are under computer control. These operations include catching a bead in the trap, determination of bead positions, allowing the molecules to flow in, attaching them between the beads (limiting the force applied to them), and releasing beads from the trap. Finally, the force applied to a molecule during an experiment can be adjusted through computer control of the flow speed and/or position of the bead in the laser trap.

Throughput of single-molecule experiments

Quantifying throughput for single-molecule experiments is difficult, because throughput is dependent on both the instrument and the experiment. Besides increasing the number of experiments that can be performed in a given time period, automation of an instrument allows the user to monitor the performed experiment without the need to control every detail. Moreover, automation increases the repeatability of the experiments, facilitates the use of the instrument, and affords a finer control and gentler manipulation of the biological system. To give an approximation of the throughput in our system, we considered the assembly of a DNA molecule between a trapped bead and a stationary surface. The combination of flow control, exchangeable beads, and automation allows us to tether a DNA between a trapped bead and a bead fixed on a pipette in ~4 min, starting from

an empty flow chamber. More significantly, the experimenter only has to fix a bead on the pipette (a procedure that takes a few seconds), while the rest of the tethering procedure is fully automated. Because the flow chamber is emptied by pushing an air bubble through it, the chamber does not have to be replaced between experiments. Therefore, the tethering can be repeated many times in an hour, and because the operator only participates during brief periods of time during the experiment, it is possible to run the instrument nearly continuously. Finally, starting the instrument, filling the pressure bottles with the desired solution, flushing the system, and calibrating it takes less than ~30 min. The combination and consistency of these procedures maximize the throughput of this instrument.

CALIBRATION AND PERFORMANCE

Position calibration

To calibrate detector output to the position of a bead in the laser trap, an increasing flow was used to displace a bead held in the trap. At each flow rate, the bead displacements were measured by video microscopy and were used to calibrate the resulting deflection measured by the photodetector (Fig. 6). This procedure is fully automated in our instrument. However, this method allows only calibration of one of the detector axes. To confirm that the photodetector has the same sensitivity in both directions we employed a second calibration method as well. A fixed bead, either adhering to the coverglass surface or attached to the tip of the micropipette, was moved in a raster pattern through the beam, using the translation stage. This method allows cal-
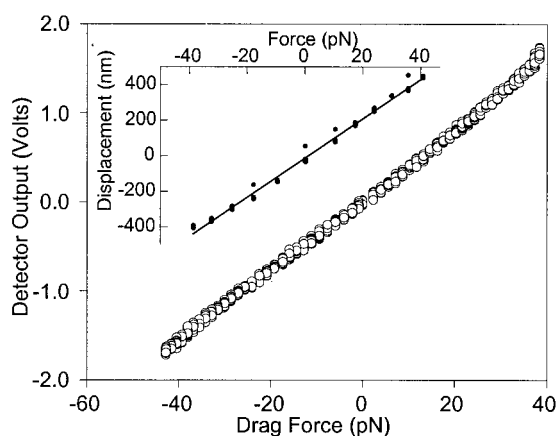

FIGURE 6   The calibration curves are taken with a 2.2-μm polystyrene bead at 178-mW laser power. The flow, which imparts a drag force on the bead, is reversed back and forth and is incrementally increased until the bead escapes the trap. The system is linear over ~400 nm. *Inset*: The displacement measurements of the bead are taken directly from the video image of the bead in the trap. The escape force of this system at 178-mW laser power is ~45 pN for a 2.2-μm-diameter bead; this value is similar to the escape forces of other single-beam optical traps.

ibration of both detector axes but needs a calibrated stage (Svoboda and Block, 1994b).

Trap stiffness calibration

Hydrodynamic drag force on a trapped particle was used to obtain a force displacement calibration for objects in the laser trap. The slope of such a calibration gives the trap stiffness. Hydrodynamic drag produced by periodic movement of the microscope stage (Ashkin, 1992; Kuo and Sheetz, 1993; Simmons et al., 1996; Wang et al., 1997) requires a well-calibrated translation stage. Here continuous flows were used instead. The drag force on a particle of known size at a known flow speed was calculated from Stokes' law. Bead displacements and the corresponding laser deflection at various flow rates were used to obtain plots of force and bead displacement versus detector output. Conversion factors from the detector output to displacement and to force were thus obtained. The stiffness of the trap was calculated from the ratio of these conversion factors. This calibration method does not require the shape of the trap to be a perfect parabolic but does rely on a position-calibrated video microscope as well as on known flow rates. Stiffness calibration is automated in our instrument, and the error in stiffness determination with this method is ultimately dictated by the accuracy with which the flow speed through the cell can be determined (see below).

The force acting on a trapped bead, its displacement in the trap, and the corresponding deflection of the laser were found to be related linearly within a region of ~400 nm from the center of the trap for a 2.2-μm bead at the maximum laser power (Fig. 6). Displacements greater than 400 nm from the center of the single-beam trap make the bead move down the optical axis as well, causing it to escape. The trap stiffness is directly proportional to the laser power. At the maximum laser power (maximum output of the diode laser 178 mW), the laser trap has an average escape force of 45 pN and an average stiffness of 110 pN/μm (Fig. 6, *inset*). The same calibration values were obtained when the corner frequency of the Brownian motion of a trapped bead was used to calibrate the stiffness (Fig. 7; Svoboda and Block, 1994a).

Flow speed calibration

Two different methods were used to determine the flow speed in the middle of the fluid chamber. In the first method, beads are passed through the chamber; the concentration is low enough (2.5×10^{-3} %, w/v) so that only a few beads are in the camera view at one time. The computer measures the time it takes for the edge of a bead to travel from one side of the field of view to the other. Because the distance of the camera view is calibrated, the speed of the bead can be calculated. This method works at relatively low
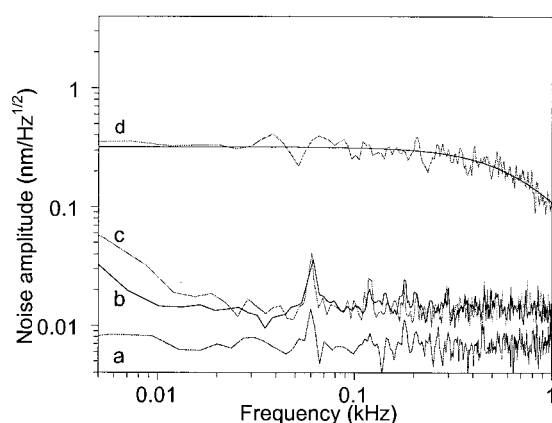
FIGURE 7 Noise power spectral density of the detector signal. The data in this plot are not normalized. (*a*) Dark noise: detector signal with no light hitting detector; (*b*) bright noise: noise of the laser beam without an object in the focal region; (*c*) fixed-bead noise: laser noise with a 2.2-μm polystyrene bead fixed to the microchamber coverglass and sitting in the focal region. The bead was fixed by drying the bead on a coverglass surface, after which water was again added to the coverslide. (*d*) Brownian motion: the power spectral density of a trapped bead. This data set is taken with a 2.2-μm bead in full laser power (178 mW). Corner frequency $f_c \approx$ 800 Hz; trap stiffness $\approx$ 105 pN/μm.

flow rates (up to 400 μm/s) and is fully automated. The error of the flow speed determination of this method is ~10%. The limitation of the flow rate arises from the fact that the CCD camera integrates the signal for 1/60 of a second. The contrast of the bead edge compared with the background is reduced when the bead moves faster, because the image of the bead is spread out over a larger area of the CCD camera. The lower contrast at higher speeds makes the computer-controlled recognition of the bead edge more difficult.

The second method of flow speed determination uses a trapped bead that is released from the trap at different flow rates by closing the shutter. The next video frame immediately after the bead is released is automatically captured by the computer. The escaped bead appears as a long streak on the video frame because of the integration time of the CCD camera (16.6 ms). The length of the streak is measured manually. The flow rate is calculated from the length of the streak and the integration time of the CCD camera. This method works well up to 1600 μm/s and has an error of ~5%. At higher flow rates the blurred bead image is not completely contained within the width of one video frame, and the flow rate cannot be determined by this method.

Instrument performance

Power spectra were compared under four different conditions: dark noise, bright noise, "fixed-bead" noise, and the Brownian motion of a trapped bead (Fig. 7). The bright noise was measured by projecting the laser light that has

passed through the instrument on the detector, and the fixed-bead noise is the detector signal created by the laser, which interacts with a bead adsorbed to the surface of the microscope chamber in the laser path.

The lower noise limit in the optical trap, represented by the dark noise, is 0.007 nm/Hz$^{1/2}$ (X_{rms} = 0.15 nm, B = 0.5 kHz); this noise is predominately electronic in origin. The noise increase between the bright noise and dark noise power spectra in Fig. 7 reflects the magnitude of the optical noise sources (largely shot noise) of the instrument. This noise increase is ~0.008 nm/Hz$^{1/2}$, resulting in a total r.m.s. value of 0.35 nm (B = 0.5 kHz). The "fixed bead" power spectrum shows a slight increase in the noise at lower frequencies due to stage drift. The noise level of ~0.015 nm/Hz$^{1/2}$ is comparable to other optical trap systems (Svoboda and Block, 1994a; Veigel et al., 1998) and is ~10-fold smaller than the Brownian motion of a trapped bead (see below). The small peak at 60 Hz in curves *a*, *b*, and *c* (Fig. 7) is caused by the A/D converter, which digitizes the detector output.

Noise due to Brownian motion of a trapped bead determines the maximum spatial resolution attainable with the instrument, given a certain bandwidth. In an actual experiment a tethered bead experiences Brownian motion similar to that of an untethered trapped bead. Between 7 Hz and 600 Hz, the Brownian motion of the trapped bead is (~0.25 nm/Hz$^{1/2}$), resulting in a r.m.s. value of 6.1 nm (B = 600 Hz). This r.m.s. value is similar to the expected value calculated from the equipartition theorem ($\alpha_{trap} \approx$ 110 pN/μm, X_{rms} = 6.2 nm).

The stiffness of a pipette is ~4 nN/μm, as determined from the equipartition theorem: $\frac{1}{2}\alpha\langle x^2 \rangle = \frac{1}{2}k_B T$, where k_B is Boltzmann's constant and T is the absolute temperature. A bead was held on the pipette tip and positioned in the center of the laser beam. The mean square displacement of the bead $\langle x \rangle^2$ obtained with the calibrated photodetector was used to calculated the pipette stiffness. Because the pipette is mechanically attached to the chamber, systematic errors like electronic noise and drift, which are present in the power spectrum of a fixed bead (Fig. 7), will be present in the noise of a bead on a pipette. Systematic sources of noise will artificially increase $\langle x^2 \rangle$ and decrease the apparent stiffness. Therefore, 4 nN/μm is a lower estimate. However, because the stiffness of the pipette is nearly two orders of magnitude larger than that of the laser trap, the pipette functions in effect as a stationary wall.

In the laminar flow mode, as for a typical experiment described by Davenport et al. (2000), when a 2.2-μm bead is held at the end of a 3.5-μm DNA molecule and extended by 5.5 pN of drag force, the experimental uncertainty in the length determination of the tether is ~11 nm (X_{rms}). This error is due to Brownian motion and the uncertainty of the centroid determination of the beads (Appendix B). Error due to drift in the microscope stage is eliminated from the measurements in this mode because the relative distance between the two beads can

be obtained with the video microscope and the two beads move simultaneously with the pipette.

TEST APPLICATIONS

Experimental setup

Two experiments, stretching DNA and monitoring the activity of single RNA polymerase molecules, are described here to illustrate the capabilities of this instrument. The majority of tasks involved in these experiments are automated and can be performed without operator intervention. An operator initiates an experiment by fixing a bead on the tip of the pipette by suction and starting the automated procedures. A dilute solution of beads is allowed to flow through the chamber, and the computer can detect when a bead has been trapped, because the drag force on a trapped bead will deflect the laser light. The instrument can automatically detect the position of beads by analyzing captured video frames. It can also differentiate between a trapped bead and a bead on the pipette by comparing the bead positions in two video frames, before and after the pipette has been moved to a different position. Once the position of the trap is known, the size of the trapped object can be determined by measuring the size of the black ring (the edge of the bead). If the laser traps multiple beads, which create an image larger than a single bead, a shutter blocks the laser light briefly to release them. The computer then continues the search for a single bead. Once a single bead is in the trap and a bead is on the pipette, the experiment can be continued. The instrument moves the pipette in front of the laser trap to shield the trapped bead and applies high flow to remove the remaining beads from the chamber. The automated positioning of the pipette uses either the pipette bead or the edge of the pipette itself as a reference to determine the position of the pipette in relation to the trap. After a set time, the flow stops and the pipette moves away from the trap. At this point, the buffer switches are set to allow the flow of the experimental materials, for example, biotinylated DNA molecules. The flow speed is increased while the force on the trapped bead is monitored, until the drag force on the bead attains a value of ∼30 pN. The fluid exchange at this flow speed is fast without risking the escape of the bead from the trap. After buffer with macromolecules is allowed to flow in for a fixed time, the computer switches back to buffer alone, and flow continues while DNA attaches to the beads. After this, the automated assembly procedure (described earlier) starts.

When a biomolecule is assembled between two beads, the instrument can be used in several modes. In the laminar flow mode, the bead positions are obtained directly from the video image. The laminar flow mode is used here in the study of RNA polymerase to avoid laser damage to the enzyme. Once the transcription complex assembly has been made, the laser beam is blocked and the free bead is extended in flow. Buffer containing nucleoside triphosphates (NTPs) is automatically allowed to flow into the chamber to initiate transcription. The load force on the molecules can then be varied by varying the flow speed. For experiments that are insensitive to laser exposure, such as stretching DNA, the bead can be retained in the laser trap, and the instrument is operated in the laser trap mode or the combined laminar/optical mode, using high laser power. When operating in these modes, we measure the bead positions by tracking the laser deflection.

Upon manual termination of the experiment by the operator, an air bubble is pushed through the chamber and fresh beads are injected. After a successful experiment the automated calibration procedure can be started (see Calibration and Performance). As a result of these preprogrammed functions, the instrument operator needs only to correct errors that cannot be solved by the computer. The few manual tasks that remain include preparing solutions of biomolecules, filling buffer bottles, and placing a bead on the tip of the pipette at the beginning of each experiment.

DNA elasticity

The elastic properties of λ DNA molecules were used to test the application of force by either the laser trap or the flow-control system The elastic properties of DNA have been well characterized (Cluzel et al., 1996; Smith et al., 1996). Linear DNA was assembled between two streptavidin-coated beads (Appendix A) by the automated assembly procedure. In the first experiment, the force on the DNA was produced using the combined laminar/optical mode. The combination of the laser trap and flow can produce forces in excess of 80 pN (Fig. 8). The DNA was stretched by moving the micropipette away from the laser trap opposite the direction of the flow, increasing the force exerted on the trapped bead. Fig. 9 shows a force-extension curve of full-length λ DNA (Fig. 9A) and a 9866-bp fragment of λ DNA (Fig. 9 *B*) in 0.5 M NaCl. As expected, both lengths of DNA undergo an overstretching transition at approximately 65 pN (Cluzel et al., 1996; Smith et al., 1996).

As an alternative to force generation with the laser trap, the laminar flow mode was also used to stretch DNA. In this experiment, the trapped bead was released from the trap after the DNA was assembled between the beads. The DNA and the previously trapped bead were then extended in the flow. This flow can provide a drag force of less than 1 pN and up to 70 pN. The flow speed was slowly ramped up and down to vary the drag force on the bead. As before, the extension of the DNA was monitored by measuring the bead positions through video microscopy. Fig. 10 shows a force-extension curve obtained by this method for a 14,771-bp DNA fragment in 0.5 M NaCl. The force on the DNA molecule was calculated from the flow speed using Stokes' law and was corrected for the hydrodynamic shielding generated by the micropipette. The DNA undergoes an overstretching transition
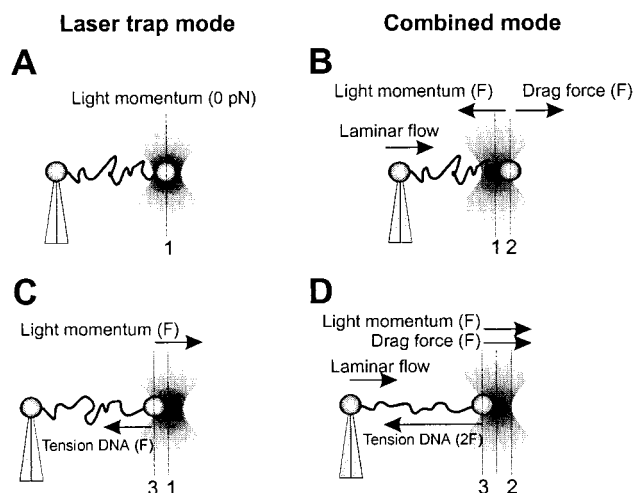
FIGURE 8 In the combined laminar/optical mode the useful range of force application by the optical trap can be doubled. (*A*) Without flow the equilibrium position of the bead in the trap is in the center of the beam (position 1). (*C*) The maximum tension that can be applied to the DNA with the optical trap is *F* (position 3). (*B*) The laminar flow creates a drag force *F* on the bead and shifts accordingly the equilibrium position of the bead in the trap to position 2. (*D*) From position 2, the laser trap can create a maximum tension in the DNA of 2*F* (position 3), twice the amount possible without the flow present.

at ~68 pN, indicating that forces exerted by either the laser trap or the flow can be determined accurately.

NTP-dependent tether-shortening by RNA polymerase

Stalled, biotinylated transcription elongation complexes were prepared (Appendix A) and assembled between streptavidin beads held on the micropipette and in the laser trap (Davenport et al., 2000); the automated assembly procedure was used to prevent irreversible stalling of the stalled complexes due to excessive force. After a stalled complex was assembled between the two beads, the trapped bead was released from the laser trap to avoid laser damage (laminar flow mode). The bead was then extended by maintaining flow, which provided a drag force of less than 15 pN. To initiate transcription, all four NTPs were allowed to flow into the fluid chamber. Upon transcription of the DNA tether, the distance separating the two beads was expected to shorten; to assay for this shortening, the positions of the two beads were measured directly from the video image. Because the flow direction is perpendicular to the optical axis and hence is in the plane of the video image, changes in tether length should directly reflect movement of RNA polymerase along the DNA (Appendix C). Fig. 11 shows an example of NTP-dependent shortening of the distance between beads tethered by a stalled transcription elongation complex. The contour length (*L*) is calculated from the end-to-end distance of the DNA (*x*) as described in Appen-
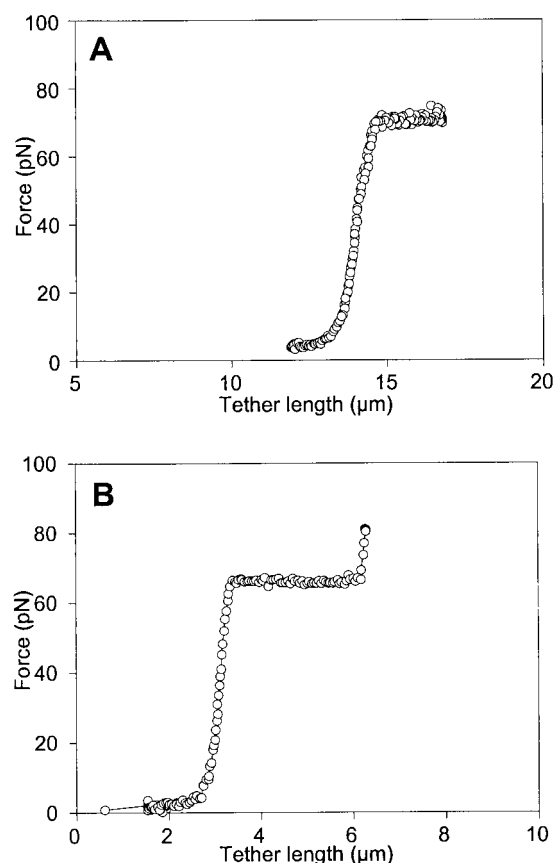

FIGURE 9 Overstretching DNA with laser trap force. DNA was assembled between two beads, using the automated assembly procedure, and stretched by stepping the micropipette away from the laser trap. Experiments were performed in 10 mM Tris-Cl (pH 8.0), 0.5 M NaCl. (*A*) Bacteriophage λ DNA (48,502 bp). (*B*) *Hin*dIII-*Bam*HI fragment of bacteriophage λ DNA (9866 bp).

dix C. Because the DNA was extended in constant flow, the experiment was performed under constant force conditions. The average peak rate measured by this method was 7.3 ± 3 bp/s (for 0.2 mM NTPs; *n* = 53), comparable to rates measured by other in vitro microscopy methods (5–20 bp/s; Schafer et al., 1991; Wang et al., 1998; Yin et al., 1994, 1995). The average time for the RNA polymerase to be transcribed in the laminar flow mode was 400 ± 250 s (*n* = 53), which is significantly longer than 82 ± 58 s when the polymerase is exposed to ~90-mW laser power, as was reported by Yin et al. (1995). Possibly free radicals are formed in the focus of the laser light. These radicals might react with and disable the RNA polymerase. Longer observation times allow transcription to be followed over thousands of base pairs, making it possible to study multiple pausing events by one molecule and/or to reveal long-lived substates of the enzyme.

CONCLUSION

As a complement to bulk biochemistry, optical trapping detection permits the investigation of the behavior of single
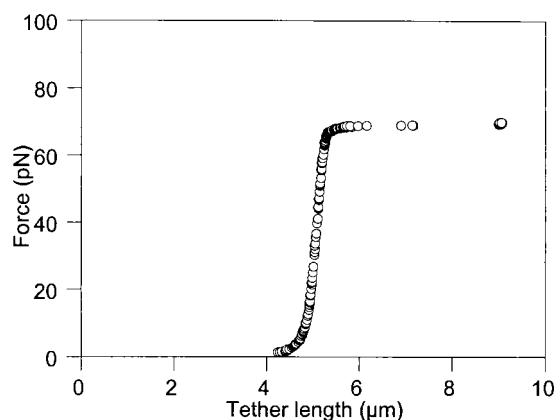
FIGURE 10 Overstretching 14,771-bp DNA with flow force. Linearized pBW8 plasmid DNA was assembled between two beads, using the automated assembly procedure. The laser-trapped bead was released from the trap and extended by flow. The DNA was stretched by ramping the flow to increase the hydrodynamic drag force.

biomolecules and the study of the effect of force on such molecules. These studies are necessarily limited by the requirement to measure one molecule at a time. Moreover, high-intensity laser light can damage some biological systems. We have developed an integrated laser trap/flow control video microscope that is automated to maximize throughput of single-molecule experiments while minimizing laser light exposure when necessary. Its various modes of operation make it possible to choose between high spatial resolution measurements or low laser exposure in single-molecule experiments. We have studied the elasticity of DNA, using either the combined laminar/optical mode or the flow control system alone (laminar flow mode) to exert the force. The stretching of DNA
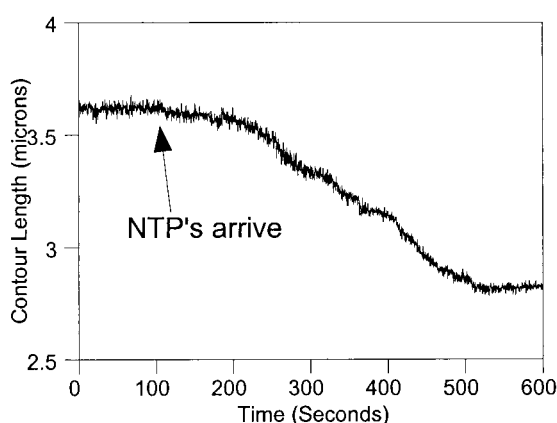

FIGURE 11 NTP-dependent tether-shortening by transcription of RNA polymerase. Stalled transcription elongation complexes were assembled between two beads by the automated assembly procedure. After successful assembly the trapped bead was released from the laser to avoid laser damage, and the DNA was extended by maintaining a flow. NTPs were allowed to flow into the chamber while the distance between the beads (x_m) was measured directly from the video image.

shows not only that the optical trap can be used as a force transducer, but that it can also be combined with the flow system and video detection to create a flexible system that can be adjusted to best suit new biological systems for study. Moreover, the extensive automation of flow control and sample manipulation allows exact repetition of experimental procedures on separate molecules, minimizes operator error, and increases experimental throughput in the instrument. Using chemically modified beads as surfaces to which molecules can be attached greatly increases the number and variety of biological systems accessible to study. This system is especially well suited to monitoring the activity of biological enzymes that translocate along or change the structure of nucleic acids in a time-dependent manner. We have shown that the laminar flow mode allows the observation of translocation by *Escherichia coli* RNA polymerase for long times and over long distances. In addition, the control of flow and buffer conditions afforded by the instrument is ideal for studying the effect of the addition or removal of buffer constituents or accessory factors that modify the system under study.

APPENDICES

A: Experimental materials

Carboxylated polystyrene microspheres (2.2-μm diameter or 3.5-μm diameter, 5% w/v; Sphero, Libertyville, IL) covalently coated with streptavidin were used in all experiments. Beads (2.5% w/v) were coated by incubation with 5 mg/ml EDAC (1-ethyl-3-(dimethylaminopropyl)carbodiimide, hydrochloride; Molecular Probes, Eugene, OR) and 0.5 mg/ml streptavidin (Gibco BRL, Gaithersburg, MD) in 5 mM sodium acetate (pH 5.1) (2 ml total volume) for 2 h with gentle shaking. Beads were washed by centrifugation at 3000 $\times$ g for 15 min, followed by resuspension in 2 ml phosphate-buffered saline. After a final centrifugation at 3000 $\times$ g for 15 min, the bead pellet was resuspended in 1 ml phosphate-buffered saline + 0.1% sodium azide (final concentration 2.5% w/v). For experiments the bead stock solution is diluted by 1:1000, and an automated syringe is used to inject exact and repeatable volumes of suspended beads (80 μl).

For development of the assembly procedure and for measurement of the elasticity of DNA, three DNA molecules were used: linearized monomers of bacteriophage λ DNA (48,502 bp); linearized pLT1 plasmid (a derivative of pBW8; Feiss et al., 1983) (14,771 bp); or a *Hin*dIII-*Bam*HI fragment of bacteriophage λ DNA (9866 bp). DNA fragments were labeled with biotinylated nucleotides by filling in 5′ overhangs from restriction endonuclease digestion. DNA (0.1 pmol) was labeled by incubation with biotin-14-dATP and biotin-14-dCTP (25 μM each) (Gibco BRL) and dGTP and dTTP (100 μM each) (Sigma) and either Exo⁻ klenow fragment of DNA polymerase I (New England Biolabs, Beverly, MA) or Exo⁻ T4 DNA polymerase (Worthington, Freehold, NJ). Labeling reactions were performed in a total volume of 60 μl.

Labeled DNA was diluted to a working concentration of 10 pM in buffer containing 10 mM Tris-Cl (pH 8.0), 500 mM NaCl, and 0.1% sodium azide. To assemble DNA between beads in the microscope, the DNA solution was allowed to flow into the chamber for 100 s at a rate that exerted a force of ~30 pN on a bead held in the optical trap. Attachment of DNA molecules to the bead can be visualized as a sudden increase in drag on the bead (Fig. 4). Typically, three to five molecules of DNA attach to the bead during the time in which the DNA flows through the chamber. The likelihood of attaching two molecules simultaneously during the fishing procedure is small; moreover, once a tether is made between the two beads and flow is lowered or halted, DNA molecules that have not

attached to both beads are not extended far enough to make an attachment. The presence of only one double-stranded molecule of DNA is verified by examining its characteristic stretching curve: a single molecule undergoes an overstretching plateau at 65–70 pN; multiple molecules will produce an overstretching transition at multiples of the single-molecule value.

For biotinylation of the transcription template, pPIA6 was linearized with *Bam*HI restriction endonuclease (New England Biolabs). Linearized plasmid (5 pmol) was incubated for 20 min at room temperature in 60 μl total volume 1× *Bam*HI buffer (New England Biolabs) containing bio-14-dATP and bio-14-dCTP (25 μM each) (GibcoBRL), dTTP and dGTP (100 μM each) (Sigma), and 0.5 μl Exo$^-$ T4 DNA polymerase (Worthington). The labeling reaction was quenched with 3 μl of 0.5 M EDTA (pH 8.0) and spun in a Microcon 100 (Amicon, Beverly, MA). The Microcon 100 was washed twice with 400 μl 10 mM Tris (pH 7.9), and the sample was recovered. The recovered sample was digested with *Sac*I restriction endonuclease (New England Biolabs) to produce a linear DNA fragment biotinylated at only one end. This DNA fragment was then gel purified on a 0.7% agarose-TAE gel and electroeluted into low TE in a dialysis bag (Spectrapor 2, 12,000–14,000 molecular weight cutoff). The eluent was extracted once with phenol/chloroform/isoamyl alcohol and once with chloroform; the DNA in the aqueous phase was precipitated with ethanol, resuspended in low TE, and stored at 4°C. (The biotinylation seems to degrade when the sample is stored at −20°C.)

Transcription complexes were stalled at position $^+$70 by incubating 10 nM linearized DNA template with 40 nM biotinylated RNA polymerase (gift of Robert Landick) in 1× transcription buffer (50 mM Tris-HCl (pH 8.0), 200 mM KCl, 10 mM MgCl$_2$, 1 mM dithiothreitol) for 10 min at 37°C; then adding 200 mg/ml Heparin, 100 μM ATP, 100 μM GTP, and 20 μM UTP; and incubating for 10 min at 25°C. Stalled complexes were diluted to a working concentration of 40 pM in 1× transcription buffer containing 1% dithiothreitol and 0.1% NaAzide.

B: Limits to the spatial resolution of video microscopy and laminar flow mode

The image of the CCD camera is calibrated with a calibration grid graduated in 10-μm increments (Nikon). Beads imaged by the CCD camera appear as light, circular objects surrounded by a black edge. The bead position is determined by averaging the positions of all of the pixels inside the circular black edge of the bead image. An image of a bead 2.2 μm in diameter typically contains ~1000 pixels (1 pixel = ~60 nm). The centroid of the bead can be calculated by averaging the *x* and *y* positions of all of the pixels:

$$X_{\text{centroid}} = \frac{\sum\limits_{n} x_n}{N} \quad \text{and} \quad Y_{\text{centroid}} = \frac{\sum\limits_{n} y_n}{N} \quad (1)$$

where x_n and y_n are the coordinates of the individual pixels and N is the total number of pixels in the image. The position uncertainty in one pixel is ±30 nm, but the standard deviation of the mean decreases with the number of pixels in the image:

$$\delta_{\text{centroid}} = \frac{\delta_{\text{pixel}}}{\sqrt{N}} \quad (2)$$

The centroid of a 2.2-μm bead image can thus be theoretically determined with an accuracy of ~1 nm (0.03 pixel). The resolution is essentially linearly related to the radius of the bead image (or the pixels on the edge of the image). It might be possible to obtain higher resolution measurements by using the exact gray values of the whole bead image. The empirically measured error in the centroid position is ~3 nm. Although the bead position can be determined, in principle, at a maximum sampling rate of 30 Hz (bandwidth of the CCD camera 60 Hz), in practice this rate is

limited to 20 Hz because of the time required to extract the distance data from the video frame. To extract data in real time, only the portion of the video frame that contains the bead images is used.

After the bead is released from the laser trap and extended by hydrodynamic drag, the Brownian motion perpendicular to the flow is greater than that along the axis of the flow, i.e., along the tether between the two beads. The theoretical error in position determination due to thermal noise can be approximated from the fluctuation-dissipation theorem (Landau and Lifshitz, 1980):

$$\bar{X}_{\text{rms}} \approx \frac{1}{\alpha_{\text{DNA}} + \alpha_{\text{trap}}} \sqrt{\frac{2k_{\text{B}}T\gamma B}{\pi}}$$

$$(\text{with } B \ll \alpha/\gamma \equiv \bar{\omega}_{\text{c}} \text{ and } \gamma = 6\pi\eta r) \quad (3)$$

where α_{DNA} and α_{trap} are the spring constants of DNA and the laser trap respectively, B is the bandwidth of the measurements in radians/s, ω_{c} is the corner frequency of the bead in the potential well, η is the viscosity of the medium, r is the radius of the bead, k_{B} is the Boltzmann constant, and T is the absolute temperature. In the laminar flow mode α_{trap} is 0 pN. The spring constant of DNA can be calculated from the expression (Bustamante et al., 1994; Marko and Siggia, 1995)

$$F = \frac{k_{\text{B}}T}{P}\left[\frac{1}{4(1-(x/L))^2} + \frac{x}{L} - \frac{1}{4}\right] \quad (4)$$

where F is the force applied to a bead tethered to a DNA molecule attached at its other end to a fixed support, P is the persistence length of DNA ($P = 53$ nm in the ionic strength conditions used in these experiments), x is the end-to-end distance at that force; and L is the contour length. The spring constant can be determined as

$$\alpha_{\text{DNA}} = \left(\frac{\partial F}{\partial x}\right)_{x\approx L} = \frac{4F^{3/2}}{L}\sqrt{\frac{P}{k_{\text{B}}T}} \quad (5)$$

The position of a 2.2-μm bead held in the laser trap ($\alpha_{\text{trap}} \approx 90$ pN/μm) in the absence of flow can be empirically determined with an accuracy of 4.6 nm (X_{rms}), using video microscopy. As expected, this error is equal to the error due to Brownian motion of the bead (Eq. 3; 1.6 nm; $B = 60$ Hz) plus the error of the centroid determination (3 nm). When a 2.2-μm bead is held at the end of a 3.5-μm DNA molecule and extended by 5.5 pN of drag force, the experimental uncertainty in position determination is 6.8 nm. The error due to Brownian motion is higher in this case, namely 3.1 nm (Eq. 5; $\alpha_{\text{DNA}} \approx 50$ pN/μm at 5.5 pN).

C: Calculation of the contour length from the bead-bead distance

The end-to-end distance of the DNA (x) is obtained by subtracting the radii of the beads (B_{corr}) from the center-to-center bead distance (x_{m}). The applied force (F), created by hydrodynamic drag by the buffer flow on the bead, was calibrated to the flow speed as described previously. The actual force applied to the molecule is the force determined by the calibration minus the drag reduction caused by the presence of the pipette. The value of such drag reduction is obtained by holding an untethered trapped bead behind the pipette at various distances and at various flow speeds. The force detection capability of the laser allows direct measurement of the hydrodynamic shielding of the pipette.

A DNA molecule displays elastic behavior when pulled by its ends. The separation between the beads gives the end-to-end distance of the DNA, which depends on the contour length of the tethered DNA and on the tension along the molecule. The contour length can be calculated from the end-to-end distance by correcting for the applied force. For forces greater that 2–3 pN, the contour length of the DNA molecule (L) is related to the

measured end-to-end distance (x) by the relationship (Odijk, 1995; Smith et al., 1992, 1996)

$$L = \frac{x}{\left(1 + \dfrac{F}{S}\right)\left(1 - \sqrt{\dfrac{k_B T}{4PF}}\right)} \tag{6}$$

where F is the force acting on the molecule and S is the stretch modulus of DNA ($\sim$1200 pN; Smith et al., 1996).

The calculated contour length, however, may differ from the real contour length, depending on the point of attachment of the complex on the pipette bead. The contour length can be corrected for the attachment location because the contour length of the DNA molecule is known. A correction factor, B_{corr}, defined as

$$B_{corr} = x_m - x \tag{7}$$

can be calculated for each data set, where x_m is the measured end-to-end distance and x is the expected end-to-end distance calculated from Eq. 6 for a DNA molecule with a known contour length. B_{corr} can then be used to correct the measured end-to-end distances in the whole data set for attachment geometry. A typical value of B_{corr} is one bead radius. The error in the calculation of B_{corr} is dependent on the error in x_m and x. The error in the end-to-end length (x), in turn, depends on the error in the force ($\sim$5–10%) applied to the DNA. x_m can be obtained more accurately by averaging the signal for a long time ($\sim$100 s). Therefore, the error in the calculation of B_{corr} is mainly dependent on the force uncertainty and is $\sim$10 nm at 5 pN (given an error of 10%).

Requests for additional information considering the instrument, the computer code, or the test experiments should be addressed to the authors.

REFERENCES

Ashkin, A. 1992. Forces of a single-beam gradient laser trap on a dielectric sphere in the ray optics regime. *Biophys. J.* 61:569–582.

Ashkin, A., and J. M. Dziedzic. 1987. Optical trapping and manipulation of viruses and bacteria. *Science.* 235:1517–1520.

Ashkin, A., J. M. Dziedzic, J. E. Bjorkholm, and S. Chu. 1986. Observation of a single-beam gradient force optical trap for dielectric particles. *Opt. Lett.* 11:288–290.

Brenner, M. 1994. *Am. Lab.* 26:14–19.

Bustamante, C., J. F. Marko, E. D. Siggia, and S. Smith. 1994. Entropic elasticity of lambda-phage DNA. *Science.* 265:1599–1600.

Cluzel, P., A. Lebrun, C. Heller, R. Lavery, J. L. Viovy, D. Chatenay, and F. Caron. 1996. DNA: an extensible molecule. *Science.* 271:792–794.

Davenport, R. J., G. J. L. Wuite, R. Landick, and C. Bustamante. 2000. Single-molecule study of transcriptional pausing and arrest by *E. coli* RNA polymerase. *Science.* 287:2497–2500.

Denk, W., and W. W. Webb. 1990. Optical measurements of picometer displacements of transparent microscopic objects. *Appl. Opt.* 29:2382–2391.

Feiss, M., I. Kobayashi, and W. Widner. 1983. Separate sites for binding and nicking of bacteriophage lambda DNA by terminase. *Proc. Natl. Acad. Sci. USA.* 80:955–959.

Finer, J. T., R. M. Simmons, and J. A. Spudich. 1994. Single myosin molecule mechanics: piconewton forces and nanometre steps. *Nature.* 368:113–119.

Ghislain, L. P., N. A. Switz, and W. W. Webb. 1994. Measurement of small forces using an optical trap. *Rev. Sci. Instrum.* 65:2762.

Ghislain, L. P., and W. W. Webb. 1993. Scanning-force microscope based on an optical trap. *Opt. Lett.* 18:1678.

Gittes, F., and C. F. Schmidt. 1998. Interference model for back-focal-plane displacement detection in optical tweezers. *Opt. Lett.* 23:7–9.

Happel, J., and H. Brenner. 1991. Low Reynolds Number Dynamics. Kluwer Academic, Dordrecht, the Netherlands.

Horowitz, P., and W. Hill. 1989. The Art of Electronics. Cambridge University Press, New York.

Kellermayer, M. S. Z., S. B. Smith, H. L. Granzier, and C. Bustamante. 1997. Folding-unfolding transitions in single titin molecules characterized with laser tweezers. *Science.* 276:1112.

Kuo, S. C., and M. P. Sheetz. 1992. Optical tweezers in cell biology. *Trends Cell Biol.* 2:116–118.

Kuo, S. C., and M. P. Sheetz. 1993. Force of single kinesin molecules measured with optical tweezers. *Science.* 260:232–234.

Landau, L. M., and E. M. Lifshitz. 1980. Statistical Physics, Pt. 1, Vol. 5. Pergamon Press, Oxford.

Lorentz, H. A. 1907. *In* Abhandlungen über Theoretische Physik, Leipzig. 23.

Ishijima, A., H. Kojima, T. Funatsu, M. Tokunaga, H. Higuchi, H. Tanaka, and T. Yanagida. 1998. Simultaneous observation of individual ATPase and mechanical events by a single myosin molecule during interaction with actin. *Cell.* 92:161–171.

Marko, J., and E. Siggia. 1995. Stretching DNA. *Macromolecules.* 28:8759.

Odijk, T. 1995. Stiff chains and filaments under tension. *Macromolecules.* 28:7016–7018.

Perkins, T. T., D. E. Smith, and S. Chu. 1997. Single polymer dynamics in an elongational flow. *Science.* 276:2016–2021.

Schafer, D. A., J. Gelles, M. P. Sheetz, and R. Landick. 1991. Transcription by single molecules of RNA polymerase observed by light microscopy. *Nature.* 352:444–448.

Simmons, R. M., J. T. Finer, S. Chu, and J. A. Spudich. 1996. Quantitative measurements of force and displacement using an optical trap. *Biophys. J.* 70:1813.

Smith, D. E., and S. Chu. 1998. Response of flexible polymers to a sudden elongational flow. *Science.* 281:1335–1340.

Smith, S. B., Y. Cui, and C. Bustamante. 1996. Overstretching B-DNA: the elastic response of individual double-stranded and single-stranded DNA molecules. *Science.* 271:795.

Smith, S. B., L. Finzi, and C. Bustamante. 1992. Direct mechanical measurements of the elasticity of single DNA molecules by using magnetic beads. *Science.* 258:1122–1126.

Svoboda, K., and S. M. Block. 1994a. Biological applications of optical forces. *Annu. Rev. Biophys. Biomol. Struct.* 23:247–285.

Svoboda, K., and S. M. Block. 1994b. Force and velocity measured for single kinesin molecules. *Cell.* 77:773–784.

Svoboda, K., C. F. Schmidt, B. J. Schnapp, and S. M. Block. 1993. Direct observation of kinesin stepping by optical trapping interferometry. *Nature.* 365:721–727.

Tskhovrebova, L., J. Trinick, J. A. Sleep, and R. M. Simmons. 1997. Elasticity and unfolding of single molecules of the giant muscle protein titin. *Nature.* 387:308–312.

Veigel, C., M. L. Bartoo, D. C. S. White, J. C. Sparrow, and J. E. Molloy. 1998. The stiffness of rabbit skeletal actomyosin cross-bridges determined with an optical tweezers transducer. *Biophys. J.* 75:1424–1438.

Visscher, K., S. P. Gross, and S. M. Block. 1996. Construction of multiple-beam optical traps with nanometer-resolution position sensing. *IEEE J. Selected Top. Quantum Electron.* 2:1066–1067.

Wang, M. D., M. J. Schnitzer, H. Yin, R. Landick, J. Gelles, and S. M. Block. 1998. Force and velocity measured for single molecules of RNA polymerase. *Science.* 282:902–907.

Wang, M. D., H. Yin, R. Landick, J. Gelles, and S. M. Block. 1997. Stretching DNA with optical tweezers. *Biophys. J.* 72:1335–1346.

Wuite, G. J. L., S. B. Smith, M. Young, D. Keller, and C. Bustamante. 2000. Single-molecule studies of the effect of template tension on T7 DNA polymerase activity. *Nature.* 404:103–106.

Yin, H., R. Landick, and J. Gelles. 1994. Tethered particle motion method for studying transcript elongation by a single RNA polymerase molecule. *Biophys. J.* 67:2468–2478.

Yin, H., M. D. Wang, K. Svoboda, R. Landick, S. M. Block, and J. Gelles. 1995. Transcription against an applied force. *Science.* 270:1653–1657.